moting adhesion with fillers or with reinforcements in composites. Finally, we note a parallel between our observations and the well-known properties of Sclair polyethylene which from the melt readily grows large spherulites with unusually regular banding; one wonders if the adventitious presence of a potent diluent is responsible for this behavior even in such an unreactive polymer.

Acknowledgment. We are grateful to Dr. J. P. Bell, University of Connecticut, for communicating results of his researches with Y. K. Choun prior to publication.

Registry No. PCL, 24980-41-4; PCL (SRU), 25248-42-4; PESUB, 25776-26-5; PESUB (SRU), 26762-06-1; PEAZ, 26760-99-6; PEAZ (SRU), 26762-07-2; PESEB, 25037-32-5; PESEB (SRU), 25034-96-2; PVC, 9002-86-2; PVP, 9003-39-8; nylon 66, 32131-17-2; nylon 610, 9011-52-3; nylon 610 (SRU), 9008-66-6.

References and Notes

(1) Briber, R. M.; Khoury, F. *Polymer* **1987**, *28*, 38.
(2) Khambatta, F. B.; Warner, F.; Russell, T. P.; Stein, R. S. *J. Polym. Sci., Polym. Phys. Ed.* **1976**, *14*, 1391.
(3) Ong, C. J.; Price, F. P. *J. Polym. Sci., Polym. Symp.* **1978**, *63*, 45.
(4) Tanaka, H.; Nishi, T. *J. Fac. Eng. Univ. Tokyo* **1983**, *A21*, 36.
(5) Tanaka, H.; Ikeda, T.; Nishi, T. *Appl. Phys. Lett.* **1986**, *48*, 393.
(6) Nojima, S.; Tsutsui, H.; Urushihara, M.; Kosaka, W.; Kato, N.; Ashida, T. *Polym. J.* **1986**, *18*, 451.
(7) Koleske, J. V. In *Polymer Blends*; Paul, D. R., Newman, S., Eds.; Academic: New York, 1978; Vol. 2, p 369.
(8) Russell, T. P.; Stein, R. S. *J. Polym. Sci., Polym. Phys. Ed.* **1983**, *21*, 999.
(9) Russell, T. P.; Koberstein, J. T. *J. Polym. Sci., Polym. Phys. Ed.* **1985**, *23*, 1109.
(10) Phillips, P. J.; Rensch, G. J.; Taylor, K. D. *J. Polym. Sci., Polym. Phys. Ed.* **1987**, *25*, 1725.
(11) Chatani, Y.; Okita, Y.; Tadakoro, H.; Yamashita, Y. *Polym. J.* **1970**, *1*, 555.
(12) Allard, D.; Prud'homme, R. E. *J. Appl. Polym. Sci.* **1982**, *27*, 559.
(13) Ong, C. J.; Price, F. P. *J. Polym. Sci., Polym. Symp.* **1978**, *63*, 59.
(14) Tanaka, H.; Nishi, T. *J. Appl. Phys.* **1986**, *59*, 1488.
(15) Spherulites in films of the blends can easily be grown to diameters approaching 1 cm and, because of their regularly spaced banding, behave like circular diffraction gratings when viewed in transmitted or reflected white light.
(16) In later experiments small areas of replica torn from the polymer surface have shown, among areas of still-attached and deformed polymer, evidence of finely scaled lamellar packing similar to that illustrated in Figure 9.
(17) Occurrence of the component peak corresponding to the larger long period in this blend is unlikely to represent a consequence of isothermal thickening, since the residence time at crystallization temperature of faster growing spherulites in the undiluted PCL was greater and did not produce evidence of such thickening.
(18) We have learned in private communication from J. P. Bell and Y. K. Choun that, from studies they have conducted of selective degradation of PCL by aqueous methylamine, the thickness of interlamellar amorphous layers remains essentially constant as X-ray long periods vary with crystallization temperature.
(19) Keith, H. D. *Macromolecules* **1982**, *15*, 114, 122.
(20) That this enhancement is real and not caused by differences of preferred orientation in two-dimensional spherulitic structures has been confirmed by chopping specimens into small particles to ensure randomization of orientation and obtaining essentially the same results. It should be noted that, even in pure PESEB, there is slight enhancement in intensity of $11\bar{2}$ relative to $11\bar{1}$ as crystallization temperature is reduced; however, changes in relative intensities induced at all crystallization temperatures by blending with PVB are substantially larger in comparison.
(21) Lovinger, A. J. *J. Polym. Sci., Polym. Phys. Ed.* **1980**, *18*, 793.
(22) Growth rates of spherulites in PESEB are relatively insensitive to the presence of PVB in small concentration; addition of 1% has virtually no effect and rates are reduced by less than 30% at a concentration of 5%.
(23) Turner-Jones, A.; Bunn, C. W. *Acta Crystallogr.* **1962**, *15*, 105.
(24) Kanamoto, T.; Tanaka, K.; Nagai, H. *J. Polym. Sci., Polym. Phys. Ed.* **1971**, *9*, 2043.
(25) Fuller, C. S.; Erickson, C. L. *J.* Am. *Chem. Soc.* **1937**, *59*, 344.
(26) An alternative approach to interpretation would be that diluents capable of dipolar interaction with crystallizing molecules might restrict reptative motions in the melt; we consider this a less promising line of inquiry, however, in view of the large changes wrought by diluents in such small concentration.
(27) Phillips, P. J. *Bull. Am. Phys. Soc.* **1988**, *33*, 248.

Small-Angle Scattering from Anisotropic Systems in the Guinier Region

Ravi F. Saraf

T. J. Watson Research Center, Yorktown Heights, New York 10598.
Received April 25, 1988; Revised Manuscript Received July 25, 1988

ABSTRACT: A general formula for scattering in the Guinier region is derived for uniaxially symmetric system in terms of the inertia of ellipsoid. It is shown that the azimuthal angle dependence of the scattering pattern is independent of the shape of the particle and depends only on the axial and lateral dimensions. A method involving double-tilt is proposed and discussed to quantitatively estimate the size when the Guinier region is difficult to access for the long axis parallel to the detector plane (e.g., voids scattering from highly drawn fibers) or in cases when the axis of symmetry cannot coincide with the detector plane (e.g., single chain scattering from planar oriented films). A family of "particle" shapes ranging from convex to concave surface is considered to quantitatively estimate the error between the actual and measured aspect ratio.

Introduction

There have been various theoretical calculations and small-angle neutron scattering (SANS) studies to estimate the aspect ratio of a single chain on deformation in the condensed state[1-8] in the past 15 years. In some cases, the data are interpreted by assuming an ellipsoidal shape[2-8] for amorphous polymer and a cylindrical shape for semicrystalline polymers[7] to estimate the molecular draw ratio, defined as the aspect ratio of a single chain. In a different type of study, estimation of shape and size of voids in high strength fibers and metallic alloys is important to determine the ultimate mechanical strength. Small-angle X-ray scatterins (SAXS) is a commonly used method for estimating void size.[10-15] The shape of the void is interpreted ellipsoidal to account for the elliptical scattering pattern (for example, ref 14 and 15). The conjecture on the shape of the scatterer from Guinier region analysis may not be valid as discussed in this paper. Other motivation for this

0024-9297/89/2222-0675$01.50/0

paper is to estimate the size and aspect ratio of the scattering species when the axis of symmetry is perpendicular to sample thickness. For example, single chain (SANS) or void (SAXS) scattering from equibiaxially deformed polymer.[16,17]

The problem of anisotropic scattering has been addressed before. Guinier and Fournet[18] address scattering from ellipsoids and cylinders, to demonstrate the applicability of Guinier's law to anisotropic objects. Kratky and Porod[19] have calculated anisotropic scattering from thin rods and cylinders. Rosse and Schull[20] and Hamzeh and Bragg[21] have interpreted anisotropic scattering by assuming the inhomogeneity as ellipsoids. In a more general treatment, the Guinier slope is interpreted as simply the projected distance average[22] based on the general equation given by Zimm.[9] However, the treatment does not provide a quantitative measurement of the molecular draw ratio. Sadler[23] proposed a formulation based on Zimm's equation where the average angle between the scattering inhomogeneities and the scattering vector is approximated as average second spherical harmonic (i.e., second-order Lagendre polynomial). In a more general treatment, Summerfield and Mildner[24] have calculated the scattered intensity in the Guinier range from a pair correlation function possessing a uniaxial symmetry. The formulation does not explicitly address the relationship between the measured Guinier slope and the "particle" shape. The correlation function approach also obscures the physical meaning of the Guinier slope (as demonstrated in the present work) and the relation between the anisotropy of the scattering pattern and the "particle". This paper demonstrates ellipsoidal symmetry of the scattering pattern in the Guinier region, as will be mentioned later in the Scattering Pattern section.

This paper estimates the error between the measured and actual anisotropy of the scattering species for uniaxially symmetric system. The method is based on a general formulation of Guinier's law expressed explicitly in terms of the shape function of the anisotropic "particle" possessing uniaxial symmetry. Here and subsequently in this paper, the scattering object, such as a single polymer chain in SANS or a void in SAXS, is refered to as a particle. A deuteriated single chain for SANS is particle-like because in the Guinier range the local structure of the chain is blurred due to large measuring length; only the chain envelope is seen. Voids are considered as particles because they are zero electron density regions embedded in finite density matrix. The formula gives a quantitative and physical interpretation to radius of gyration measured from any arbitrary azimuthal angle of the scattering pattern. The relationship between the slope of the Guinier plot and radius of gyration, establishes a correspondence between the particle shape and the measured Guinier slopes at arbitrary azimuthal angle. On the basis of this formulation a method involving double tilt of the sample is proposed to estimate the size and anisotropy of the scattering particle.

Scattering Optics

Figure 1 shows the optics of the scattering experiment. The sample is located at O, and O-XYZ is the coordinate system defining the optics. The X-ray beam is incident parallel to the Y axis, and the detector is parallel to X–Z plane. The sample's axis of symmetry defined by unit vector $\hat{n}$ is located by angles γ and ψ with respect to O-XYZ, the lab frame of reference, where γ is the *first* tilt around the X axis (at $\psi = 0$) and ψ is the *second* tilt around the Z axis. Also note the directions of the two tilts: at $\gamma = \psi = 0$, $\hat{n} \parallel Z$ axis; at $\gamma = \pi/2$ and $\psi = 0$, $\hat{n} \parallel +Y$ axis;

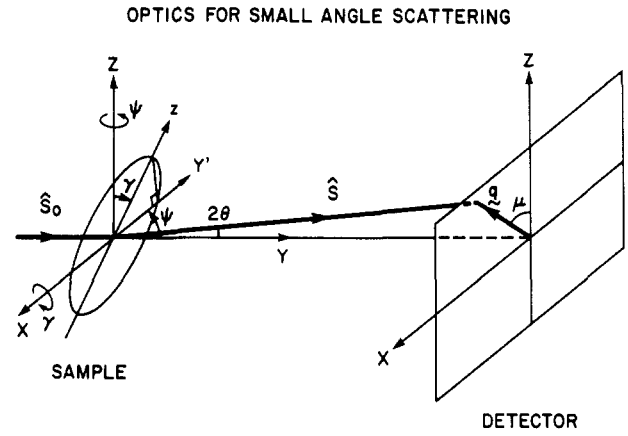

Figure 1. In the small-angle scattering experiment, the incident beam is parallel to the $+Y$ axis and the detector is parallel to the X–Z plane. The sample is located at O. The unique axis of the sample, defined as the z axis, is the axis of symmetry. The sample is first tilted by γ around the X axis, followed by second tilt of ψ around the Z axis. The directions of the two tilts are as indicated.

at $\gamma = \psi = \pi/2$, $\hat{n} \parallel -X$ axis. The incident and the scattered beam are defined by unit vectors $\hat{s}_0$ and $\hat{s}$, respectively. Then, with respect to O-XYZ coordinate system

$$\hat{s}_0 = \hat{J} = (0,1,0)$$

$$\hat{s} = -(\sin 2\theta \sin \mu)\hat{I} + (\cos 2\theta)\hat{J} + (\sin 2\theta \cos \mu)\hat{K} = (-\sin 2\theta \sin \mu, \cos 2\theta, \sin 2\theta \cos \mu) \quad (1)$$

Therefore the scattering vector $\mathbf{q}$ is given by

$$\mathbf{q} = \frac{2\pi}{\lambda}(\hat{s} - \hat{s}_0) = \frac{2\pi}{\lambda}(-(\sin 2\theta \sin \mu)\hat{I} + (\cos 2\theta - 1)\hat{J} + (\sin 2\theta \cos \mu)\hat{K}) \quad (2)$$

$$\Rightarrow \quad q = \frac{4\pi}{\lambda} \sin \theta$$

For small-angle scattering, the scattering angle 2θ is very small. Thus, $1 - \cos 2\theta \approx 0$. Therefore, from eq 2, the scattering vector $\mathbf{q}$ has only X and Z components. In other words, the Ewald sphere for small-angle scattering is a plane and is parallel to the X–Z plane in these optics.

Guinier Region

The amplitude of the scattered beam $A_s(\mathbf{q})$ is given by

$$A_s(\mathbf{q}) = \int dV\, \rho_0 e^{i\mathbf{qr}} \quad (3)$$

where ρ_0 is the density of the particle, $\mathbf{r}$ is the position vector of the elemental volume dV (see Figure 2). Assuming constant density ρ_0 and denoting x_q as the component of $\mathbf{r}$ along $\mathbf{q}$

$$A_s(\mathbf{q}) = \rho_0 \int dV\, e^{iqx_q}$$

Since, in the Guinier region, $qx_q \ll 1$, the higher order terms of the exponential expansion can be neglected to give

$$A_s(\mathbf{q}) = \rho_0 \int dV\, [1 + iqx_q - \tfrac{1}{2}(qx_q)^2]$$

Since the scattered intensity $I_s(\mathbf{q})$ is $A_s(\mathbf{q})\, A_s^*(\mathbf{q})$, Guinier's law becomes

$$I_s(\mathbf{q}) = \rho_0 V^2[1 - q^2\langle x_q^2\rangle] \quad (4)$$

where

$$\langle x_q^2\rangle = \int dV\, x_q^2/V \quad (5)$$

The term $q^2\langle x_q\rangle^2$ in eq 4 vanishes by assuming the particle

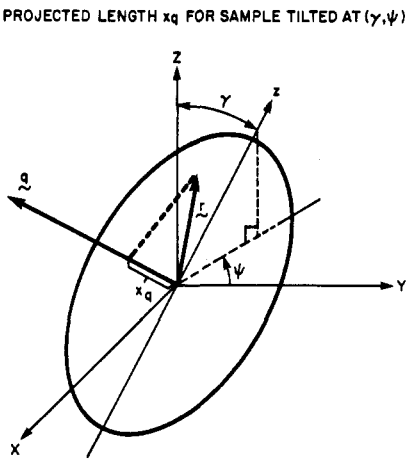

Figure 2. Projected length x_q defined as the component of **r** along the q axis. The q axis along **q** defines the Ewald sphere and is parallel to the detector plane, X–Z. The slope of the Guinier plot is equal to $\langle x_q^2 \rangle$ and is defined by eq 5.

to be centrosymmetric. This equation is the Zimm equation.[9] The information on the size and shape of the particle is in the slope and azimuthal dependence of the Guinier plot $(I_s(\mathbf{q})/(\rho_0 V^2)$ versus $q^2)$. The value of $\rho_0 V^2$ is obtained by extrapolating to $q = 0$.

The measured $\langle x_q^2 \rangle$ can be expressed in terms of the radii of gyration of the particle as follows. Let O-xyz be the natural coordinate system of the particle, such that z axis $\parallel \hat{n}$. Let the direction cosines of **q** in O-xyz coordinate system be cos α, cos β, and cos γ with respect to the x, y, and z axes, respectively. Thus

$$x_q = \mathbf{q}\cdot\mathbf{r}/q = x \cos\alpha + y \cos\beta + z \cos\gamma \tag{6}$$

By substituting eq 6 in eq 5, adding and subtracting r^2, and rearranging

$$\langle x_q^2 \rangle = R_r^2 - [(\cos\alpha)^2 R_x^2 + (\cos\beta)^2 R_y^2 + (\cos^2\gamma) R_z^2] \tag{7}$$

where the respective radii of gyration are defined as

$$R_r^2 \equiv \langle r^2 \rangle$$
$$R_x^2 \equiv \langle y^2 + z^2 \rangle$$
$$R_y^2 \equiv \langle x^2 + z^2 \rangle$$
$$R_z^2 \equiv \langle x^2 + y^2 \rangle \tag{8}$$

The average quantities in eq 8 are defined similar to $\langle x_q^2 \rangle$ (see eq 5).

The Guinier's law in eq 4 can be interpreted in two ways. From eq 5, the slope in the Guinier region is the average of the square of projected length x_q. This interpretation was utilized by Sadler.[23] The second interpretation is given by eq 7. Here the slope is indeed equal to R_r^2 minus square of the projected radius of gyration. What is important to note in eq 7 is that $\langle x_q^2 \rangle$ is equal to the inertia of ellipsoid at the centroid of the particle (except for a constant R_r^2). Thus the measured slope as a function of α, β, and γ will resemble the shape of the body. Therefore, in principle, from Guinier's law in eq 5, it should be possible to estimate the approximate shape of the scattering particle, i.e., the aspect ratio.

Projected Radius of Gyration

A general body of revolution is assumed, to quantify eq 7 and hence the Guinier's law. Consistency of this formulation is later demonstrated by assuming isotropic, cylindrical, and ellipsoidal particles to obtain the well-known Guinier's formulas.

The centrosymmetric and uniaxially symmetric particle in its natural coordinates O-xyz can be defined by

$$x^2 + y^2 = f^2(z) \tag{9}$$

where

$$f(z) = f(-z)$$

where $f(z)$ defines the shape of the particle. Note that $f(z)$ is not necessarily a bounded function of z. However, in the present case, $f(z) = 0$ for $|z| > l$.

In O-xyz frame of reference, eq 8 gives

$$R_r^2 = \frac{8}{V}\int_0^l \int_0^{f(z)} \int_0^{(f^2(z)-y^2)^{1/2}} dx\, dy\, dz\, (x^2 + y^2 + z^2) \tag{10a}$$

$$\Rightarrow R_r^2 = \frac{\pi}{V}\int_0^l dz\, [f^4(z) + 2f^2(z)z^2]$$

Similarly

$$R_x^2 = \frac{\pi}{2V}\int_0^l dz\, [f^4(z) + 4f^2(z)z^2] \tag{10b}$$

$$R_y^2 = \frac{\pi}{2V}\int_0^l dz\, [f^4(z) + 4f^2(z)z^2] \tag{10c}$$

$$R_z^2 = \frac{\pi}{V}\int_0^l dz\, f^4(z) \tag{10d}$$

where the particle volume is given by

$$V = 2\pi \int_0^l dz\, f^2(z) \tag{11}$$

Substituting eq 10a–d and 11 in eq 7, the Guinier plot slope becomes

$$\langle x_q^2 \rangle = \frac{\left[\frac{\pi}{2}\sin^2\gamma \int_0^l dz\, f^4(z) + \pi \cos^2\gamma \int_0^l dz\, f^2(z)z^2\right]}{2\pi \int_0^l dz\, f^2(z)} \tag{12}$$

The next step is to determine the angle γ between the z axis (the sample axis of symmetry) and the q axis parallel to the X–Z plane (i.e., the detector plane). From the definition of the two tilt angles (see Figure 1), the Z component of z axis is $z \cos\gamma$; and the X component is $z \sin\gamma(-\sin\psi)$. Note that $-\sin\psi$ is due to the definition of the direction of rotation of the second tilt by ψ. Since the z axis component along the q axis is $z \cos\gamma$

$$\cos\gamma = -\sin\psi \sin\gamma \sin\mu + \cos\gamma \cos\mu \tag{13}$$

Substituting eq 12 and 13 in eq 4, the scattering in the Guinier region is given as

$$\frac{I_s(\mathbf{q})}{\rho_0 V^2} = 1 - q^2[A \sin^2\gamma + B \cos^2\gamma] =$$
$$1 - q^2[(B - A)\sin^2\psi \sin^2\gamma \sin^2\mu + (B - A)\cos^2\gamma \times \cos^2\mu - (B - A)\sin\psi \sin 2\gamma \sin\mu \cos\mu + A] \tag{14}$$

where

$$A = \frac{\pi}{2V}\int_0^l dz\, f^4(z)$$
$$B = \frac{\pi}{V}\int_0^l dz\, f^2(z)z^2 \tag{14'}$$

Equation 14 is the scattering equation in the Guinier region for scattering from an anisotropic system with uniaxial symmetry. As mentioned earlier, l can tend to infinity. Thus the applicability of the equation is more general. In the next section the shape of the scattering pattern is

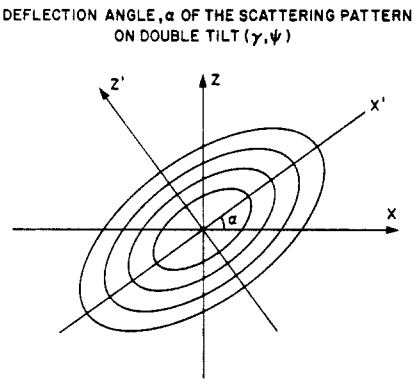

Figure 3. Scattering pattern deflected by angle α on tilting the sample by (γ,ψ) (defined in Figure 1). The angle of deflection is independent of the scattering particle shape, size, and aspect ratio. It depends only on the tilt angles as shown in eq 17.

considered by evaluating the locus of the isointensity lines on the two-dimensional detector.

For a spherical particle of radius l, $f^2(z)$ and $l^2 - z^2$. Substituting this functionality in eq 14′ and integrating, $A = B = l^2/5$. Thus, Guinier's law for a spherical particle by eq 14 becomes

$$\frac{I_s(\mathbf{q})}{\rho_0 V^2} = 1 - \frac{1}{3}q^2R_g^2 \tag{15}$$

where R_g^2 is the polar radius of gyration of a sphere and is given by $R_g^2 = {}^3/_5 l^2$. Thus eq 14 leads to a consistent result for isotropic condition.

Scattering Pattern

Consider a constant-intensity line measured on the two-dimensional detector. Since $1 - I_s(\mathbf{q})/(\rho_0 V^2) = K$ is a constant, the locus of the isointensity line in the Guinier region is given by (using eq 14)

$$\left[\frac{B-A}{K}\sin^2\psi\sin^2\gamma\right]q^2\sin^2\mu + \left[\frac{B-A}{K}\cos^2\gamma\right]q^2\cos^2\mu + \left[-\frac{B-A}{K}\sin\psi\sin 2\gamma\right]q^2 \times \sin\mu\cos\mu + \frac{A}{K}q^2 = 1 \tag{16}$$

It is obvious from eq 16 that the scattering pattern is not symmetric about the X and Z axis. The pattern after doublt-tilt rotates anticlockwise by an angle α (Figure 3). By simple transformation from the X–Z to the Z'–Z' frame the angle of rotation is given by (see Appendix)

$$\tan 2\alpha = \frac{\sin\psi\sin 2\gamma}{\cos^2\gamma - \sin^2\psi\sin^2\gamma} \tag{17}$$

Equation 17 implies that *the deflection of the scattering pattern by double tilt is independent of the particle shape.*

It is obvious from eq 16 that for an isotropic case (i.e., spherical particle) the contour lines are circular because $A = B$. For $\gamma = \pi/2$ and $\psi = 0$, eq 16 yields circular contour lines. This is also as expected, because the axis of symmetry is parallel to the incident beam (see Figure 1).

Another important condition to note is that of no tilt, i.e., $\gamma = \psi = 0$. From eq 13, $\gamma = \mu$ for the no tilt condition. Then the contour lines in the Guinier region become (according to eq 16)

$$\frac{A}{K}q^2\sin^2\mu + \frac{B}{K}q^2\cos\mu = 1 \tag{18}$$

Equation 18 indicates that the locus is an ellipse irrespective of the shape of the particle. Thus, the scattering pattern for any uniaxially symmetric particle is always elliptic. This result has been reported earlier by using a pair correlation function approach to calculate the scattered intensity in the Guinier region.[24] This point could also be deduced from the second interpretation of Guinier's law, i.e., the $\langle x_q^2\rangle$ is similar to ellipsoid of inertia. When the axis of symmetry coincides with the Z axis, the projected radius of gyration has only $\cos^2\mu$ and $\sin^2\mu$ terms (see eq 7 and 6). Therefore, the shape of the scattering species cannot be inferred from the two-dimensional scattering pattern in the Guinier region. This further implies that the anisotropy measured by the Guinier slopes may not be the actual anisotropy of the chain from SANS data[2,6,8] or of the void from SAXS data.[10,13-15] This discrepancy will be considered later in the paper.

Tilt Optics

Equation 16, for a single tilt, $\psi = 0$ and $\gamma \neq 0$, leads to

$$\frac{A}{K}q^2\sin^2\mu + \frac{A\sin^2\gamma + B\cos^2\gamma}{K}q^2\cos^2\mu = 1 \tag{19}$$

Equation 19 indicates the pattern remains elliptic after a single tilt. The apparent radius of gyration along the Z axis (i.e., $\mu = 0$) is changed to $A\sin^2\gamma + B\cos^2\gamma$.

The application for Guinier scattering for arbitrary tilt may have application in the systems mentioned below. For single chain scattering (SANS) from highly oriented polymers, such as gel spun[25,26] and hydrostatic deformed[27,28] high-density polyethylene, a large deformation ratio leads to a large anisotropy. Therefore, the Guinier region parallel to the draw axis may be obscured under the beam stop. The problem in SAXS from voids in highly oriented fibers made by wet spinning of liquid-crystalline polymer dope may be similar.[29] In all these systems, the sample tilt be tilted to pull-out the Guinier region to wider angles. The apparent Guinier slope for single tilt will become (see eq 19)

$$\text{slope}_X^{ST} = A$$

$$\text{slope}_Z^{ST} = (B - A)\cos^2\gamma + A \tag{20a}$$

Similarly, the apparent Guinier slope for double tilt will become (see eq iv in the Appendix)

$$\text{slope}_X^{DT} = (B - A)\sin^2\psi\sin^2\gamma + A$$

$$\text{slope}_Z^{DT} = (B - A)\cos^2\gamma + A \tag{20b}$$

In a single tilt, slope_X^{ST} remains unchanged, but slope_Z^{ST} is attenuated depending on the angle γ. In a double tilt, both the slopes decrease (as expected); slope_Z^{DT} becomes the same as slope_Z^{ST}. If γ is less than $\pi/4$, then slope_X^{DT} is attenuated more than slope_Z^{DT}. Thus double tilt offers an advantage over single tilt. The major axis to minor axis ratios of the isointensity contour lines for single and double tilt are given by eq 19 and iv (Appendix) respectively as

$$R^{ST} = 1 + \frac{B-A}{A}\cos^2\gamma$$

$$R^{DT} = \frac{C_1\cos^2\alpha + C_2\sin^2\alpha + {}^1/_2C_3\sin 2\alpha}{C_1\sin^2\alpha + C_2\cos^2\alpha - {}^1/_2C_3\sin 2\alpha}$$

For efficient use of the counting time, the choice of tilt angles should be such that the Guinier region extends to larger scattering angles and the ellipticity of the pattern (i.e., R^{ST} and R^{DT}) is kept as large as possible. The exact conditions will depend on the property of the sample (i.e., A/B, physical dimensions of the sample that may limit the

tilt angles) and the optics (i.e., lower limit on the measurable scattering angle).

Simple shear deformation of a single chain has been studied by SANS.[8] In this study, the principle direction of stretching is calculated by assuming simple shear.[8] However by the above formulation this angle can be directly determined by measuring the angle of deflection of the pattern given by eq 17. In one sample measured by these tilt optics, the calculated and measured shear angle differ by only 5%.[16]

The double tilt method may also be suitable for thin-film samples where the axis of symmetry is parallel to the thickness direction. Examples of such systems are single chain SANS from equibiaxially deformed polymer[16,17] and void scattering from biaxially stretched semicrystalline and rigid-rod polymer films.[17,30] It should be mentioned that single-tilt method in small-angle light scattering has been utilized for characterizing spherulitic crystal growth morphology in poly(ethylene oxide) (thin) films.[31]

Limitation of Guinier Scattering

A major limitation of Guinier scattering is that the shape of the scattering species cannot be determined. This is apparent in the general formula given by eq 14, where the only sample parameters obtained are A and B. Although A and B are related to the particle shape, the integral equation relating $f(z)$ to the measurable parameters A and B has infinitely many solutions. Thus no estimation of the shape can be made from scattering measurement in the Guinier region. The ratio of Guinier slope parallel and perpendicular to the draw axis is proportional to the actual aspect ratio (defined as $l/f(0)$) of the scattering species, i.e., deformed polymer chains, voids, etc. However, the proportionality constant may differ significantly with shape for the same aspect ratio, $l/f(0)$. This discrepancy between the actual and measured aspect ratio is considered next.

Let the laterial dimension $f(0)$ be a. Then the aspect ratio of the particle is l/a. In general

$$l/a = K(B/A)^{1/2} \tag{21}$$

where the proportionality constant K will depend on the functionality of $f(z)$. For an ellipsoidal shape (using eq 14′)

$$f^2(z) = a^2[1 - (z/l)^2] \tag{22}$$

$$\Rightarrow \quad A = a^2/5 \qquad B = l^2/5$$

$$\Rightarrow \quad K = 1$$

Thus, the measured and actual aspect ratio are equal for an ellipsoidal particle. A more general particle shape may be given by

$$f(z) = a[1 - (z/l)^n] \tag{23}$$

The shape function $f(z)$ spans a wide range of particle shapes: for $n = 0$, $f(z)$ is a straight line, giving a conical shape to the particle; for $n > 1$, the particle surface is convex; for $n < 1$, the particle surface is concave (see Figure 4). The Guinier slopes A and B can be calculated by substituting eq 23 in eq 14′ to obtain

$$A = \frac{3n^2}{(4n + 1)(3n + 1)}a^2 \tag{24}$$

$$B = \frac{(2n + 1)(n + 1)}{3(2n + 3)(n + 3)}l^2$$

Thus, substituting eq 24 in eq 21 leads to

$$\frac{l}{a} = \left[\frac{9n^2(2n + 3)(n + 3)}{(n + 1)(2n + 1)(3n + 1)(4n + 1)}\right]^{1/2}\left(\frac{B}{A}\right)^{1/2} \tag{25}$$

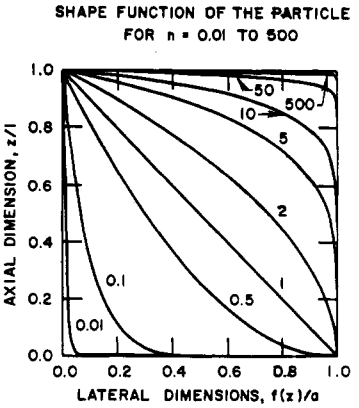

Figure 4. Shape function $f(z)$ defined by eq 9 and 23, spanning from concave (for $n < 1$) to convex (for $n > 1$) particle shapes. The three-dimensional particle is defined by rotating the area under the curve around the z axis and reflecting the resultant volume on the base plane perpendicular to the z axis at $z = 0$. For $n = 0$, the shape is a one-dimensional object along the z axis, and for $n \to \infty$ the particle is a cylinder.

On the basis of eq 25, an error between the measured and actual aspect ratio can be calculated as

$$E = \frac{(l/a) - (B/A)^{1/2}}{(B/A)^{1/2}} = \left[\frac{9n^2(2n + 3)(n + 3)}{(n + 1)(2n + 1)(3n + 1)(4n + 1)}\right]^{1/2} - 1 \tag{26}$$

Thus, $E(B/A)^{1/2}$ is the amount *underpredicted* by the measurement.

The two interesting limits of the shape function defined in eq 23 are $n \to 0$ and $n \to \infty$. In the former limit, the particle becomes a one-dimensional object of length l and zero lateral dimension. In the latter limit, the particle becomes a finite size cylinder, with length l and diameter a. For $n = 0$ (by eq 24) $A = 0$ and $B = l^2/27$. The corresponding scattering pattern becomes a "thin streak" along the X axis on the detector (given by eq 14 and 18). This formula may be useful for thin long voids, formed in high-strength fiber, where it may be possible to calculate the void length as $3(3^{1/2})B$. On the other hand, for $n \to \infty$, $A = a^2/4$ and $B = l^2/3$. (Note that this corresponds to a cylinder.) Thus the corresponding error $E = -0.134$, i.e., actual l/a is 13.4% lower than the measured aspect ratio $(B/A)^{1/2}$. Figure 5 shows the percent error defined by eq 26 as a function of the shape function index n (given by eq 23). The error ranges from −100% (at $n = 0$) to 23% (at $n = 0.854$), and the asymptotic limit for $n \to \infty$ is 13.4%. Furthermore, the error is zero (similar to ellipsoid as indicated in eq 22) for $n = 0.2586$ and 6.3348. The two shape functions correspond to a concave and a convex shape. Figure 6 shows the three shape functions (for zero error) that scatter identically in the Guinier range.

For the simplest case, where the particles are perfectly oriented, the measured slopes A and B are the sixth moment average of the (characteristic length)^2 (since $I_s(\mathbf{q}) \sim V^2$). The measured aspect ratio will be dominated by the particles with the largest NV^2, where N is the number fraction. The problem of course becomes more nondeterministic when the size, aspect ratio, orientation, and shape distributions are invoked. A misorientation of the scattering species around the sample unique axis will rotate their respective patterns according to eq 17. The deflection of the scattering pattern will depend only on the orientation distribution function and not on the shape and size of the scattering species. The total scattering pattern will tend to broaden off the X axis. The effect would be a

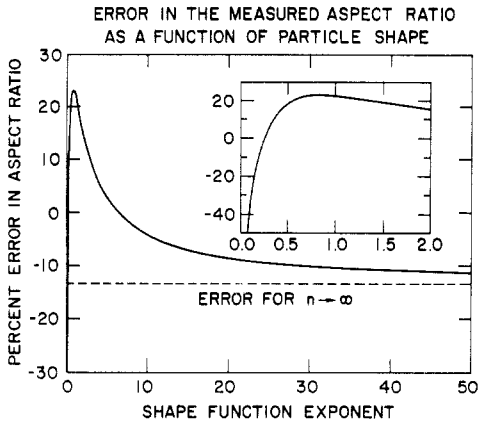

Figure 5. Percent error between the actual and the measured aspect ratio by Guinier plot plotted against the shape function index n. The error E and index n are defined in eq 26 and 23, respectively. The asymptotic line for $n \rightarrow \infty$ corresponds to -13.4%.

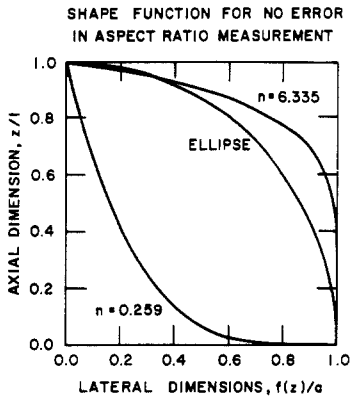

Figure 6. Particle with ellipsoidal shape corresponding to shape function index n = 0.259 and 6.335 with zero error. Note that both concave and convex shape particle can lead to zero error.

nonelliptic pattern and/or the apparent aspect ratio will appear smaller. The latter effect can clearly be visualized for random orientation of anisotropic particles. In this case the pattern is circular. Thus the effect of orientation distribution is similar to a reduction of the aspect ratio.

One possible scheme to estimate the shape of the particle is by analyzing the deviation from the Guinier's law. This will come from the next order term, i.e., $\langle qr \rangle^4$ in eq 4. This fourth average term will lead to a higher order average of $f(z)$, which puts a constraint on the choice of shape function $f(z)$. The application of such a scheme will require a high count in the Guinier region to determine the deviation from Guinier's law accurately.

Conclusion

A formula for scattering from a uniaxially symmetric particle in the Guinier region is derived. The equation relates the measured Guinier slope for any arbitrary tilt to some average size dimensions parallel and perpendicular to the axis of symmetry. The azimuthal dependence of the scattered intensity is independent of the particle shape and depends only on the axial and lateral dimensions. The scattering pattern is elliptical for any particle shape, given by shape function $f(z)$. The deflection angle of the pattern on double tilt is independent of the size, shape, and the aspect ratio of the scattering particle. It only depends on the orientation angles. An estimation of error for the aspect ratio obtained by the Guinier plot is given for a family of particle shapes. The shapes range from a thin one-dimensional object to a finite size cylinders. The estimated error for a cylindrical particle is -13.4%, for ellipsoids is zero, and for a thin long one-dimensional object is ~-100%. The error for convex shaped particles lies between ~25 and -15%.

Appendix: Calculation of the Pattern Deflection Angle α

Let

$$C_1 = \frac{B-A}{K}\sin^2\psi\sin^2\gamma + \frac{A}{K}$$

$$C_2 = \frac{B-A}{K}\cos^2\gamma + \frac{A}{K} \qquad \text{(i)}$$

$$C_3 = \frac{-(B-A)}{K}\sin\psi\sin 2\gamma$$

Substituting eq i in eq 16 and setting $X = q\sin\mu$, $Z = q\cos\mu$, the equation of the contour lines on the detector plane becomes

$$C_1X^2 + C_2Z^2 + C_3XZ = 1 \qquad \text{(ii)}$$

The transformation from X-Z to X'-Z' axes is given by (see Figure 3)

$$\begin{pmatrix} X \\ Z \end{pmatrix} = \begin{pmatrix} \cos\alpha & -\sin\alpha \\ \sin\alpha & \cos\alpha \end{pmatrix}\begin{pmatrix} X' \\ Z' \end{pmatrix} \qquad \text{(iii)}$$

Thus, the transformed equation becomes

$$[C_1\cos^2\alpha + C_2\sin^2\alpha + \tfrac{1}{2}C_3\sin 2\alpha]X'^2$$

$$[C_1\sin^2\alpha + C_2\cos^2\alpha - \tfrac{1}{2}C_3\sin 2\alpha]Z'^2 \qquad \text{(iv)}$$

$$[-C_1\sin 2\alpha + C_2\sin 2\alpha + C_3\cos 2\alpha]X'Z' = 1$$

Since the pattern is symmetric in the X'-Z' frame, the coefficient of $X'Z'$ is 0. Thus the tilt angle is

$$\tan 2\alpha = \frac{C_3}{C_1 - C_2} \qquad \text{(v)}$$

Registry No. Neutron, 12586-31-1.

References and Notes

(1) Benoit, H.; Dupplessix, R.; Ober, R.; Daoud, M.; Cotton, J. P.; Farnoux, B.; Jannink, G. *Macromolecules* **1974**, *8*, 451.
(2) Hadziioannou, G.; Wang, L.-H.; Stein, R. S.; Porter, R. S. *Macromolecules* **1982**, *15*, 880.
(3) Ullman, R. *J. Chem. Phys.* **1979**, *17*, 436.
(4) Ullman, R. *ACS Symp. Ser.* **1982**, 193.
(5) Wignall, G. D.; Wu, W. *Polym. Commun.* **1983**, *24*, 354.
(6) Sadler, D. M.; Odell, J. A. *Polymer* **1980**, *21*, 479.
(7) Ballard, D. G. H.; Cheshire, P.; Janke, E.; Nevin, A.; Schelten, J. *Polymer* **1982**, *23*, 1875.
(8) Lefebvre, J. M.; Escaig, B.; Coulson, G.; Picot, C. *Polymer* **1985**, *26*, 1807.
(9) Zimm, B. H. *J. Chem. Phys.* **1948**, *16*, 1093.
(10) Bragg, R. H.; Hammond, M. L.; Robinson, J. C.; Anderson, P. L. *Nature (London)* **1963**, *200*, 557.
(11) Fourdeux, A.; Perret, R.; Ruland, W. First International Conference on Carbon Fibers, Plastic Institute, 1971; p 71.
(12) Johnson, D. J. First International Conference on Carbon Fibers, Plastic Institute, 1971; p 52.
(13) Dobb, M. G.; Johnson, D. J.; Majeed, A.; Saville, B. P. *Polymer* **1979**, *20*, 1284.
(14) Schwahn, D.; Kesternich, W.; Schuster, H. *Metall. Trans. A* **1981**, *12*, 155.
(15) Boss, S.; Bragg, R. H. *J. Appl. Phys.* **1978**, *49*, 2916.
(16) Saraf, R. F.; Lefebvre, J. M.; Porter, R. S.; Wignall, G. D. *Scattering, Deformation, and Fraction in Polymers*; Material Research Society: Pittsburgh, 1987; Vol. 79, p 263.
(17) Saraf, R. F.; Porter, R. S. *J. Rheol.* **1987**, *31*, 59.
(18) Guinier, A.; Fournet, G. *Small Angle Scattering of X-rays*; Wiley: New York, 1955; p 26.
(19) Kratky, O.; Porod, G. *J. Colloid Sci.* **1949**, *35*, 35.
(20) Roess, L. C.; Shull, C. G. *J. Appl. Phys.* **1947**, *18*, 308.
(21) Hamzeh, F. M.; Bragg, R. H. *J. Appl. Phys.* **1974**, *45*, 3189.
(22) Sadler, D. M.; Barham, P. J. *J. Polym. Sci., Polym., Phys. Ed.* **1983**, *21*, 309.
(23) Sadler, D. M. *J. Appl. Crystallogr.* **1983**, *16*, 519.

(24) Summerfield, G. C.; Mildner, D. F. R. *J. Appl. Crystallogr.* **1983**, *16*, 384.
(25) Frank, F. C.; Keller, A.; Mackley, M. R. *Polymer* **1971**, *12*, 468.
(26) Pennings, A. J.; Schouteten, C. J. H.; Kiel, A. M. *J. Polym. Sci., Polym. Symp. Ed.* **1972**, *38*, 167.
(27) Kanamoto, T.; Tsuruta, A.; Tanaka, K.; Takeda, M.; Porter, R. S. *Polym. J.* **1983**, *15*, 327.
(28) Kanamoto, T.; Tsuruta, A.; Tanaka, K.; Takeda, M.; Porter, R. S. *Macromolecules* **1988**, *21*, 470.
(29) Cohen, Y.; Thomas, E. L. *Macromolecules* **1988**, *21*, 436.
(30) Flood, J. E.; White, J. L.; Fellers, J. F. *J. Appl. Polym. Sci.* **1982**, *27*, 2965.
(31) Hashimoto, T.; Todo, A.; Kawai, H. *J. Polym. Sci., Polym. Phys. Ed.* **1973**, *11*, 149.

Small-Angle Neutron Scattering from Star-Branched Polymers in the Molten State

J. C. Horton, G. L. Squires,* A. T. Boothroyd,† L. J. Fetters,‡ A. R. Rennie,§ C. J. Glinka,⊥ and R. A. Robinson‖

Cavendish Laboratory, Madingley Road, Cambridge CB3 0HE, U.K.
Received March 22, 1988; Revised Manuscript Received July 8, 1988

ABSTRACT: We have investigated the structure of a number of linear and star-branched polyethylene molecules, with arm numbers ranging from 3 to 18, by small-angle neutron scattering. Measurements were made in the melt at a temperature of 140 °C. Our measurements show that the Benoit scattering function, based on a random-walk model, gives an extremely good fit to the neutron scattering data, but the molecules are swollen with respect to a simple Gaussian conformation. The swelling is consistent with a model of an impenetrable core from which the arms of the star diffuse outward.

Introduction

The properties of branched polymers often differ markedly from those of linear polymers of the same molecular weight, and there is an obvious need to correlate the properties of these polymers with the type and degree of branching. Both natural and man-made samples of polymers often consist of mixtures of branched and unbranched molecules, with a wide range of molecular weights, frequency of branches, and segment length between branch points. Such diversity poses problems for interpreting the properties of the material, and theoretical models usually deal with simple branched structures. The simplest type of branching is that of star branching, where a number f of linear chains with equal numbers of monomers N are joined at a single branch point. We have measured the mean-squared radius of gyration $\langle S^2 \rangle$ by small-angle neutron scattering (SANS) for stars in the melt for a range of arm numbers and arm lengths.

It was suggested by Flory[1] in 1949 that linear polymers in the melt have a Gaussian or "random-walk" conformation. This was confirmed by SANS measurements in the early 1970s,[2] which showed that $\langle S^2 \rangle$ is proportional to N. However, it is to be expected that star molecules will show some departure from Gaussian behavior due to packing constraints near the branch point and that such departure will be most significant for molecules with a large number of short arms.

Experiment

The material used in our experiments was polyethylene. The stars were made in polybutadiene form by one of us (L.J.F.[3]). The arms were prepared, with low polydispersity ($M_w/M_n \approx 1.05$), by anionic polymerization. Polybutadiene prepared in this way has about 19 vinyl groups per thousand carbon atoms.[4] The star was formed by linking the arms to a chlorosilane core (Figure 1). From each polybutadiene star we prepared two forms of polyethylene by a catalytic reaction in which the double bond is saturated with either deuterium, to give a labeled molecule, or with hydrogen, to give an unlabeled molecule, thus

$$—[CH_2CH{=}CHCH_2—] + D_2 \rightarrow —[CH_2CHDCHDCH_2—]$$

$$—[CH_2CH{=}CHCH_2—] + H_2 \rightarrow —[CH_2CH_2CH_2CH_2—]$$

The process is described elsewhere.[5,6] After they were dried, the samples were tested for saturation by examining their infrared spectrum to check the absence of the 967-cm^{-1} absorption line. Doi et al.[7] have noted (though for a different catalyst than ours) that this is the last line to disappear during the saturation of polybutadiene.

The molecular masses of the polybutadiene stars were determined by gel permeation chromatography (GPC). The saturated materials were also checked by GPC, and the mass distributions of the protonated and deuteriated products were found to be very similar; the M_w values differed by less than 5%.

For each star a blend was prepared by mixing together approximately equal masses of the deuteriated and protonated materials in cyclohexane under reflux. This was done in a nitrogen atmosphere to prevent the polymers from being oxidized in solution, where they are particularly vulnerable to attack. Neutron measurements were made both for the blended sample and for a blank sample provided by a protonated material alone. The latter gives a measure of the incoherent scattering from the protons in the blended sample.

For an elastic scattering process the magnitude of the change in the wavevector of the neutron is

$$Q = \frac{4\pi}{\lambda} \sin \frac{1}{2}\theta \qquad (1)$$

where λ is the wavelength of the neutron and θ is the scattering angle. The neutron scattering measurements were made on the small-angle scattering spectrometer at the National Bureau of Standards at Gaithersburg[8] and on D17 at the Institut Laue-Langevin.[9] The measurements at the NBS were made with a sample–detector distance of 3.6 m and with incident wavelengths of 0.50 and 0.75 nm. These gave respective Q ranges of 0.14–1.6 nm^{-1} and 0.09–1.0 nm^{-1}. On D17 the detector was 2.8 m from the sample and was offset by an angle of 3° from the direction of the incident beam. The incident wavelength was 1.2 nm, giving a Q range of 0.13–0.9 nm^{-1}.

For both spectrometers the position-sensitive detector has a Cartesian grid of detecting elements. The scattering in the present

† Present address: Department of Physics, University of Warwick, Coventry CV4 7AL, U.K.
‡ Corporate Research Science Laboratories, Exxon Research and Engineering Company, Clinton Township, Annandale, NJ 08801.
§ Institut Laue-Langevin, 156X, 38042 Grenoble Cedex, France.
⊥ National Bureau of Standards, Gaithersburg, MD 20899.
‖ Los Alamos Neutron Scattering Center, Los Alamos National Laboratory, Los Alamos, NM 87545.

0024-9297/89/2222-0681$01.50/0